JACS
JOURNAL OF THE AMERICAN CHEMICAL SOCIETY
pubs.acs.org/JACS
Article

Anhydride Post-Synthetic Modification in a Hierarchical Metal–Organic Framework

Shoushun Chen,[#] Zhongxin Song,[#] Jinghui Lyu, Ying Guo, Bryan E. G. Lucier, Wilson Luo, Mark S. Workentin, Xueliang Sun,[*] and Yining Huang[*]

Cite This: J. Am. Chem. Soc. 2020, 142, 4419–4428
Read Online
ACCESS | Metrics & More | Article Recommendations | Supporting Information

ABSTRACT: Metal–organic frameworks (MOFs) are important porous materials. Post-synthetic modification (PSM) of MOFs via the pendant groups or secondary functional groups of organic linkers has been widely used to introduce new or enhance existing properties of MOFs for various practical applications. In this work, we have constructed, for the first time, a novel platform for PSM of MOFs by introducing an anhydride functional group into a hierarchically porous MOF (MIL-121) as an effective anchor. We have demonstrated that the combination of the high reactivity of anhydride and hierarchical porosity makes this protocol particularly novel and important, as it led to excellent opportunities of incorporating not only a wide variety of organic molecules with different sizes and chemical nature but also the noble metal complexes in MOFs. Specifically, we show that the anhydride group decorated in the MOF exhibits a high reactivity toward covalently binding 10 different guest molecules including alcohols, amines, thiols, and noble metal (Pt(II)/Pt(IV)) complexes, whereas the hierarchical pores created in the MOF allow the incorporation of guest species varying in size from methanol to larger molecules such as polyaromatic amines. This novel approach provides the community with a new avenue to prepare MOF-based materials for targeted applications. To illustrate this point, we furnish an example of using this new platform to prepare a Pt-based electrocatalyst which shows excellent catalytic activity toward the oxygen reduction reaction (ORR), a pivotal half-reaction in hydrogen–oxygen fuel cells and other energy storage and conversion devices.

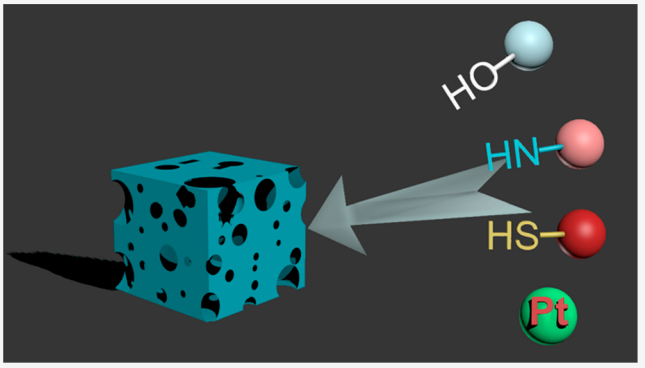

INTRODUCTION

In the past two decades, metal–organic frameworks (MOFs) have emerged and grown as the largest branch of porous materials,[1] leading to numerous new materials with many applications including gas storage,[2,3] gas separation,[4] catalysis,[5−7] chemical sensing,[8] drug delivery,[9,10] electrochemical energy storage and conversion.[11] MOFs are crystalline materials in which metal ions/clusters are connected via organic linkers to form three-dimensional porous frameworks. The robust structure and functionalization potential of organic components allow one to introduce diverse chemical functionalities into MOFs through post-synthetic modification (PSM) while keeping the overall MOF topology intact.[12,13] PSM has been employed as a general approach to improve the existing properties of and introduce new features to MOFs, with examples including enhancing framework stability to moisture, increasing gas adsorption capability, and introducing new catalytic sites.[13,14]

Among post-synthetic methods for MOFs,[13,14] covalent modification of organic linkers via a pendant group of the linker or second functional group has been employed as an efficient approach.[12−14] Although reported MOF entries in the Cambridge Structural Database (CSD) have surpassed 70,000,[15] the available functional groups as targets for PSM are mainly limited to organic species such as amino groups, hydroxyl groups, catechols, thiocatechols, 2,2′-bipyridyl moieties, etc.[13,14,16] The types of MOFs that are suitable for PSM are also limited. Factors limiting MOF selection for PSM include the stability of the MOF, as in order to maintain the MOF topology and avoid severe structural damage, the MOF candidate for PSM must be chemically robust. Preferred MOFs for PSM are typically microporous zirconium MOFs due to their chemical stability, such as UiO-66/67 and related materials.[13] The pore size of MOFs is another key factor of concern for PSM.[14] Most MOFs have micropores with pore diameters less than 2 nm, which in many cases limits the mass transfer in the channels and prevents the incorporation of large guest molecules.[14] For PSM considerations, it is important for

Received: December 12, 2019
Published: February 9, 2020

https://dx.doi.org/10.1021/jacs.9b13414
J. Am. Chem. Soc. 2020, 142, 4419–4428

MOFs to have sufficiently large pores that can encapsulate the targeted guest species for desired applications.

Anhydrides are stable but reactive carboxylate derivatives that are widely used in organic synthesis for making covalent bonds. For example, they are typically used for acetylation of alcohols and amines in organic synthesis.[17] Although decorating MOFs with pendant anhydride groups via free carboxylic acid groups on the linkers has been reported,[18,19,33,34] to the best of our knowledge, anhydride formed inside hierarchically porous MOFs has not been used as an anchor for PSM. In the present work, we demonstrate, for the first time, that an anhydride grafted inside a MOF with a hierarchical pore system can be used as a novel functional handle for PSM. The MOF chosen to highlight the efficacy of anhydride functionality for PSM is MIL-121, an aluminum-based MOF incorporating the low-cost linker precursor 1,2,4,5-benzenetetracarboxylic acid, H_4BTEC. This MOF features two "free" uncoordinated carboxylic acid (COOH) groups directed toward the interior of the channels, since only two of the four COOH groups in the BTEC linker are coordinated to the metal centers (Scheme 1).[18] These uncoordinated COOH groups occupy interior volume; thus, MIL-121 has a limited pore aperture[18] and very small Brunauer–Emmauer–Teller (BET) surface area. Very recently, we reported that the formation of anhydride groups and creation of a hierarchical pore system within MOF MIL-121 can be achieved simultaneously in a controlled fashion via thermolysis.[19]

Scheme 1. Depiction of the Conversion from Microporous MIL-121 to a Hierarchically Porous MOF with Decorated Anhydride Groups under a High Temperature of 440 °C in the Air[a]

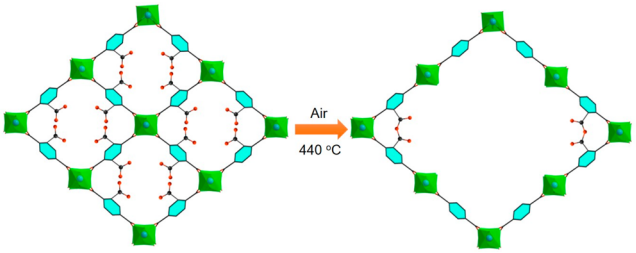

[a]During thermal treatment, the local structure partly collapses, yielding expanded pores. Concomitantly, the dangling free carboxylic acid groups pointing toward the interior of the channel are condensed to form anhydride groups. Color code: black, C; red, O; and the center green octahedron represents AlO_6.

In the present PSM study, using novel platform built on the thermally treated hierarchically porous MIL-121 (termed HMIL-121) decorated with anhydride, we have successfully grafted 10 different organic/inorganic species in HMIL-121. Specifically, we demonstrate that the combination of reactive anhydride groups and a hierarchical pore system permits immobilization of a variety of organic molecules, including alcohols, amines, and thiols, ranging in size from small molecules such as methanol to relatively large organic compounds such as polyaromatic amines. We also show that an inorganic Pt complex, tetraamine platinum hydroxide, can also be successfully incorporated into HMIL-121, demonstrating that anhydrides formed in the MOF pores can be used not only for introduction of a variety of organic moieties but also for metalation with noble metals. These PSM processes only require a one-step treatment, and the Pt complex incorporation proceeds at room temperature in water without any added catalyst, showing that the anhydride is an effective PSM anchor site. HMIL-121 has been functionalized via anhydride groups with a variety of organic and inorganic compounds and thoroughly characterized using nitrogen adsorption isotherms, powder X-ray diffraction (PXRD), scanning electron microscopy (SEM), X-ray photoelectron spectroscopy (XPS), and ^{1}H, ^{13}C, and ^{195}Pt solid-state NMR (SSNMR) spectroscopy. The information obtained in this study unlocks a better understanding of the chemistry underlying the PSM process. To demonstrate the potential for using the PSM protocol described in this work to prepare MOF-based materials with practical applications, we employ a treatment to transform the above-mentioned Pt-loaded HMIL-121 to a conductive electrocatalyst that exhibits excellent catalytic activity toward the oxygen reduction reaction (ORR).

EXPERIMENTAL SECTION

Sample Preparation. MIL-121 was prepared based on a previously reported procedure with some modifications.[18] A mixture of 1.80 g of $Al(NO_3)_3{\cdot}9H_2O$ (Alfa Aesar, 98%) and 0.60 g of pyromellitic acid (1,2,4,5-benzenetetracarboxylic acid (BTEC), Alfa Aesar, 96%) was dissolved in 10.0 mL of deionized H_2O. After stirring the reagent mixture for 10 min, 0.5 mL of 4.0 M HCl was added. After stirring for another 5 min, the mixture was placed in a Teflon chamber within a Teflon-lined stainless steel autoclave. The autoclave was then sealed and heated in an oven at 210 °C for 16 h. After cooling the autoclave to room temperature, a white powder of as-made MIL-121 was obtained by centrifugation and dried in an oven at 90 °C for 5 h.

Solvent Exchanged MIL-121. According to ref 18, the pores of as-made MIL-121 contain unreacted linkers from MOF synthesis. Therefore, a methanol (MeOH)-based solvent exchange procedure was carried out to remove unreacted BTEC ligands. A mixture of 0.20 g of as-made MIL-121 and 20.0 mL of methanol was placed into a Teflon container within a Teflon-lined stainless steel autoclave, which was then heated in an oven at 150 °C for 24 h. Upon cooling, the MeOH solvent was decanted and replaced with fresh MeOH. This solvent exchange process was repeated twice every 24 h. The final product was then dried in an oven at 90 °C for 1 h and referred to as MIL-121.

Hierarchically Porous MIL-121. Hierarchically porous MIL-121 was obtained by following the documented procedure:[19] a MIL-121 sample was placed in an oven at 440 °C and heated for 16 h. During this process, decarboxylation occurred and some metal centers were eliminated from the framework, creating hierarchical pores inside the MOF featuring grafted anhydride groups. The resulting MOF is termed as HMIL-121, which was then used as the starting material for post-synthetic modification (PSM).

Acetylation (i.e., Esterification) by Alcohols. The esterification of HMIL-121 decorated with anhydride groups via methanol is described here in detail as an example. The acetylation details of the rest of the compounds can be found in the Supporting Information.

MeO-HMIL-121. A mixture of 200.0 mg of HMIL-121 and 10.0 mL of 99.9% MeOH (Fisher Chemical) was placed in a 25 mL round-bottom flask, and then, three drops of concentrated H_2SO_4 (98%, ACP chemicals) were added. The reagent mixture in a flask was heated in an oil bath at 60 °C. The reaction was held for 5 h under magnetic stirring. The product was isolated by centrifugation. To remove residual MeOH, the sample was immersed within 25 mL of DI water and stirred for 5 min in a 50.0 mL centrifuge tube. This washing process was repeated three times before the collected product was dried at 90 °C. The dried sample was completely activated at 150 °C under a dynamic vacuum (≤1 mbar) for ca. 8 h; the fully activated final product is termed as MeO-HMIL-121.

https://dx.doi.org/10.1021/jacs.9b13414
J. Am. Chem. Soc. 2020, 142, 4419–4428

Powder X-ray Diffraction (PXRD). PXRD patterns were recorded on an Inel CPS powder diffractometer operating using Cu Kα radiation (λ = 1.5406 Å). The reflections were collected at 2θ values ranging between 5 and 120° using an increment of 0.02°.

N_2 Adsorption Measurements. N_2 adsorption isotherms were measured using a Micromeritics ASAP 2020 porosity analyzer at a temperature of 77 K.

Electron Microscopy. All SEM images were taken on a scanning electron microscope (Hitachi S-4800) operating at 5 kV. TEM samples were prepared by drop-casting an ultrasonicated solution of dilute high-performance liquid chromatography grade methanol solution with the sample of interest onto a lacey carbon grid. TEM and high-resolution TEM (HRTEM) images were taken on a JEOL 2010F Transmission Electron Microscope equipped with an energy dispersive spectrometer (EDS).

Thermogravimetric Analysis (TGA). TGA was carried out on a TA Instruments Q50 thermogravimetric instrument under N_2 flow (40 mL·min^{-1}) with heating from 40 to 800 °C at a rate of 10 °C·min^{-1}.

ICP-OES. The Pt loading level in HMIL-121-900 was determined by inductively coupled plasma-optical emission spectroscopy (ICP-OES). A 10.0 mg portion of Pt-HMIL-121-900 was dispersed in 10.0 mL of aqua regia (HCl:HNO_3 = 3:1) to completely dissolve Pt nanoparticles dispersed in the MOF-based matrix overnight. Then, 1.0 mL of aqua regia with dissolved Pt was diluted with 9.0 mL of H_2O and the resulting solution was used to measure the Pt concentration by ICP-OES. From ICP analysis, the Pt loading in Pt-HMIL-121-900 was determined to be 7.0 wt %.

SSNMR Measurement. All ^{1}H, ^{13}C, and ^{195}Pt SSNMR experiments were performed at a magnetic field of 9.4 T using a Varian InfinityPlus wide-bore NMR spectrometer.

^{13}C and ^{1}H SSNMR Spectroscopy. ^{13}C and ^{1}H SSNMR spectra [$\upsilon_0(^{13}C)$ = 100.5 MHz, $\upsilon_0(^1H)$ = 399.5 MHz] were referenced to TMS using adamantane as a secondary reference. Specifically, the high-frequency ^{13}C signal at 38.57 ppm and the ^{1}H resonance at 1.85 ppm were used for the secondary referencing.[20,21] ^{1}H−^{13}C cross-polarization magic angle spinning (CP/MAS) experiments were performed with proton decoupling and a spinning frequency of 14 kHz using a spectral width of 100 kHz, along with a ^{1}H 90° pulse length of 4.5 μs, a contact time of 7 ms, and a recycle delay of 3 s. ^{1}H MAS experiments were performed at a spinning frequency of 14 kHz and a spectral width of 100 kHz, utilizing a 90° pulse of 4.5 μs and a recycle delay of 2 s. For each ^{1}H spectrum, four scans were collected. The number of scans for each ^{13}C spectrum is listed as follows, in the format of sample:number of scans: MeO-HMIL-121:4785; EtO-HMIL-121:7785; 2-PE-HMIL-121:6897; MeNH-HMIL-121:3768; aniline-HMIL-121:6163; *p*-toludine-HMIL-121:8794; 4-ABP-HMIL-121:4308; 1-AP-HMIL-121:9428; EDT-HMIL-121:4578.

Static ^{1}H−^{195}Pt BRAIN-CPMG SSNMR Measurements. A 1.0 M aqueous Na_2PtCl_6 solution was used as a chemical shift reference ($\upsilon_0(^{195}Pt)$ = 85.59 MHz, δ_{iso} = 0.0 ppm).[22] The ^{195}Pt spectra of the two samples (i.e., $Pt(NH_3)_4(OH)_2$ and Pt-HMIL-121) were acquired using the BRAIN-CPMG pulse sequence[23] with WURST-80 excitation pulses[24,25] and ^{1}H decoupling. The ^{1}H 90° pulse length was 3.75 μs, and a contact time of 7 ms was used. The CP (cross-polarization)−WURST sweep range was 500 kHz. The ^{1}H−^{195}Pt spectra of the two samples were produced by coaddition of several individual subspectra due to the wide spectral breadth. The ^{1}H−^{195}Pt BRAIN-CPMG spectrum of the Pt salt, $Pt(NH_3)_4(OH)_2$, was assembled by the coaddition of eight subspectra. For each subspectrum, the pulse delay employed was 3 s, the spectral window was 1000 kHz, spikelet separation in the frequency domain was 5000 Hz, and the number of scans was 500. The ^{195}Pt spectrum of Pt-HMIL-121 was constructed from the coaddition of three subspectra; for each subspectrum, the pulse delay was 0.165 s, the spectral window was 1000 kHz, the spikelet separation in the frequency domain was 9090 Hz, and the number of scans was 219,992.

Electrochemical Measurements. The electrochemical characterization was performed in a three-electrode system using a rotating-disk electrode (RDE) setup with an Autolab electrochemistry station and rotation control (Pine Instruments). The ink was prepared by mixing 3.0 mg of catalyst in 3.0 mL of aqueous solution containing 0.6 mL of isopropyl alcohol and 30 μL of Nafion (5.0 wt %). Thirty min of sonication was conducted to ensure good dispersion and wetting of the catalyst. A 60 μL portion of the catalyst ink was pipetted onto a polished glassy carbon electrode (Pine, 5.0 mm dia., 0.196 cm^2) and allowed to dry at room temperature. All electrochemical measurements were carried out in 0.1 M $HClO_4$ electrolyte using a Pt wire as a counter electrode and a reversible hydrogen electrode (RHE) as a reference electrode. All potentials reported henceforth are vs RHE. Each electrode was activated by scanning from 0.05 to 1.1 V at 50 mV·s^{-1} in N_2-saturated 0.1 M $HClO_4$ solution until no change was observed in the cyclic voltammetry (CV) curves. O_2 was then bubbled into the $HClO_4$ solution for 30 min to achieve an O_2-saturated electrolyte. ORR linear sweep voltammetry (LSV, 10 mV·s^{-1}) was conducted in O_2-saturated 0.1 M $HClO_4$ solution on the RDE system with a rotation speed of 1600 rpm. The LSV curves obtained under N_2 were subtracted from the LSV curves obtained under O_2 to remove the non-Faradaic current. For comparison, the commercial 40% Pt/C catalyst was prepared on the electrode using a similar procedure as described above with a Pt loading of 10 mg·cm^{-2}. The kinetic current was calculated from the ORR polarization curves by using mass-transport correction and normalized to the loading amount of Pt in order to compare the mass activity of different catalysts. The calculations were based on the Levich−Koutecky equation[26]

$$1/i = 1/i_k + 1/i_d$$

where i_k is the kinetic current and i_d is the diffusion-limiting current.

RESULTS AND DISCUSSION

Preparation and Characterization of the Materials Used for PSM: Hierarchically Porous MIL-121 Decorated with Anhydride Groups. The protocol for preparing hierarchically porous MIL-121 decorated with anhydride functional groups via thermolysis was described in ref 19, and details are given in the Experimental Section and the Supporting Information. The hierarchial pores in MIL-121, including the pore size and pore volume, can be finely tuned by controlling the thermolysis temperature and duration. In the present study, unless stated otherwise, all of the hierarchically porous MIL-121-based materials with anhydride groups used for PSM were obained by thermolysis of MIL-121 at 440 °C for 16 h, as we have found the materials prepared under these conditions have the largest BET surface areas. Hereafter, these products are referred to as HMIL-121.

The N_2 adsorption isotherm of a typical HMIL-121 sample is shown in Figure S1a. The type IV isotherm indicates the existence of mesopores. The calculated Brunauer−Emmett−Teller (BET) surface area is 887.6 m^2/g, including a microporous area of 623.8 m^2/g and a mesoporous area of 263.8 m^2/g. The material has an average pore size of 5.20 nm. The pore size distribution in HMIL-121 was also calculated by the density functional theory (DFT) method and is shown in Figure S1b, further confirming that mesopores are present in this MOF. The SEM image of the HMIL-121 sample (Figure S1d) features mesopores of various sizes. The existence of anhydride groups in HMIL-121 is directly confirmed by ^{13}C solid-state NMR (SSNMR) spectroscopy, which will be discussed later.

Modification of HMIL-121 with Alcohols and Aromatic Amines. Nine different organic functional moieties and one platinum complex [methanol (MeOH), ethanol (EtOH), 2-phenylethanol (2-PE), methylamine ($MeNH_2$), aniline, *p*-toluidine, 4-aminobipenyl (4-ABP), 1-aminopyrene (1-AP),

https://dx.doi.org/10.1021/jacs.9b13414
J. Am. Chem. Soc. 2020, 142, 4419−4428

1,2-ethyldithiol (EDT), and tetraamineplatinum(II) hydroxide] have been successfully immobilized inside the pores of HMIL-121 (Figure 1). The PSM procedures for introducing

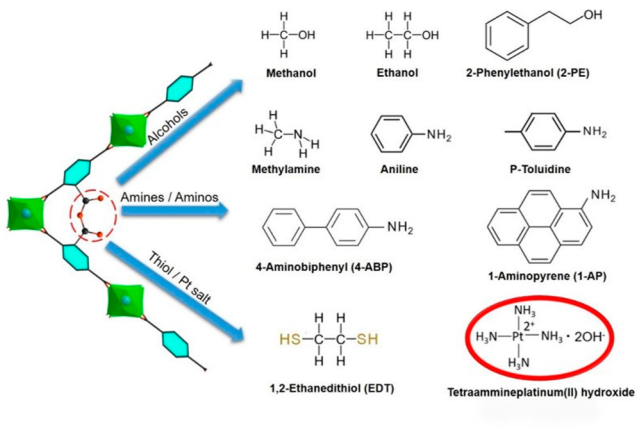

Figure 1. Illustration of the reactivities of anhydride groups in HMIL-121 toward different organic compounds and a platinum salt (O, red; C, black; Al, blue).

each guest species were individually optimized based on the chemical nature of each guest. The resulting PSM variants are termed in the format of "grafted species-HMIL-121"; e.g., MeO-HMIL-121 corresponds to HMIL-121 functionalized by methanol with a methoxy group as the grafted species. Details of PSM procedures can be found in the Experimental Section and the Supporting Information. The powder X-ray diffraction (PXRD) patterns of HMIL-121 variants functionalized by PSM are very similar to pristine HMIL-121 (Figure S2), suggesting the long-range order and topology of the MOF are preserved after PSM. The N_2 gas adsorption isotherms of HMIL-121 and its PSM variants are given in Figure 2. The N_2 adsorption capacities of modified HMIL-121 variants all significantly decreased versus the parent HMIL-121 MOF, which results from reduced pore size/space due to the existence of incorporated guest species. This decrease in N_2 uptake is a clear marker of successful guest introduction into HMIL-121 via reaction with anhydride groups.

The pore size distributions in MIL-121, HMIL-121, and post-synthetically modified HMIL-121 variants have been calculated from the N_2 adsorption isotherms via the DFT method and are shown in Figure S3. The pore size distribution of MIL-121 indicates that there are very little micropores or mesopores in the sample. This near absence of MIL-121 porosity is due to the steric hindrance of its dangling free carboxylate groups, which occupy and block the pores.[18,19] The DFT calculation indicates that, after thermal treatment, HMIL-121 features two different groups of pores: micropores with a size distribution centered around 15 Å and mesopores ranging from 20 to 500 Å. Large molecules like *p*-toluidine prefer to be "grafted" inside the mesopores, leading to a dramatically decreased mesoporous pore volume (Figure S3). In contrast, when small molecules such as $MeNH_2$ are introduced within modified HMIL-121, there is significantly decreased pore volume in both the microporous and mesoporous regions (Figure S3). It is apparent that the large molecules readily react with the anhydrides decorated in the mesopores, while the anhydride groups in the micropores of HMIL-121 are much less accessible to many guests.

To directly characterize the new functionalities introduced via PSM and gain key information on the underlying chemistry of the PSM procedures, SSNMR spectroscopy was employed. SSNMR is sensitive to local structure, provides nuclide specific information complementary to that obtained from X-ray-diffraction-based methods,[27,28] and is a proven avenue for monitoring PSM processes.[29,30] Before NMR measurements, any residual reactants that might be occluded inside the MOF

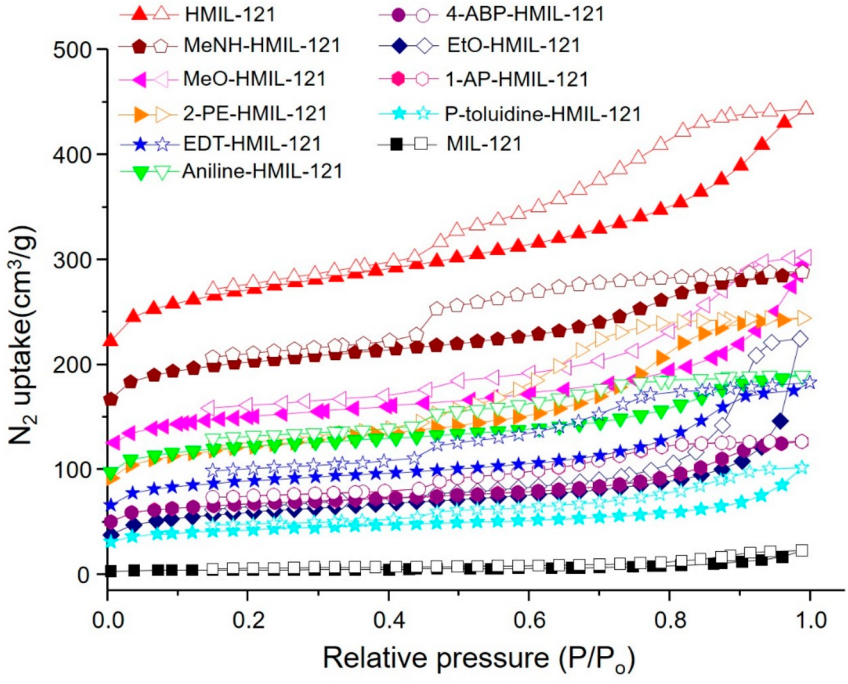

Figure 2. N_2 adsorption−desorption isotherms of MIL-121, HMIL-121, and post-synthetically modified HMIL-121 variants at 77 K. Solid circles represent adsorption and open circles denote desorption measurement points.

https://dx.doi.org/10.1021/jacs.9b13414
J. Am. Chem. Soc. 2020, 142, 4419−4428

pores were removed by thoroughly washing the sample with suitable solvents, followed by activation at high temperature and under dynamic vacuum. Only the characterization of PSM products obtained by acetylation of alcohols and amines, as well as the reaction of the Pt complex with anhydride groups anchored inside HMIL-121, is described here in detail to illustrate how the anhydride groups act to immobilize guests inside HMIL-121. The procedures for functionalizing HMIL-121 with other guests are provided in the Supporting Information.

Acetylation is a reaction that is widely used for producing many industrially important compounds, including aspirin, fatty acid esters, and macrolides.[17,31] Acetylation of an alcohol or amine with anhydride results in two products: an ester or amide, along with the corresponding acid as a byproduct (Figure 3a). Proper identification of the ester or amide fragment and corresponding acid group formed during PSM is a key step to unambiguously confirming that the acetylation occurs inside HMIL-121.

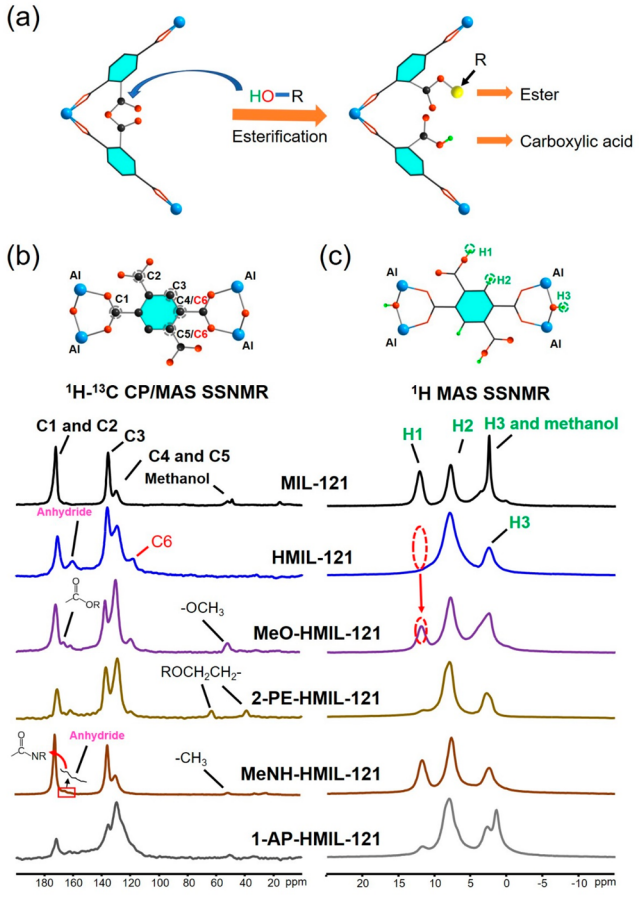

Figure 3. (a) An illustration of the esterification of an anhydride group in HMIL-121 with an alcohol, where oxygen is red, carbon is gray, aluminum is blue, and hydrogen is green. In parts b and c, the ^{13}C CP/MAS and ^{1}H MAS SSNMR spectra of MIL-121, HMIL-121, and post-synthetically modified HMIL-121 are shown. All of the spectra were obtained at a magnetic field strength of 9.4 T and a spinning speed of 14.0 kHz. In this figure, "2-PE" represents 2-phenylethanol and "1-AP" is shorthand for 1-aminopyrene. A depiction of the BTEC linker with corresponding labels for each unique carbon and hydrogen is shown at the top of each spectral stack.

To this end, ^{13}C CP (cross-polarization)/MAS (magic angle spinning) and ^{1}H MAS NMR spectra of MIL-121, HMIL-121, MeO-HMIL-121, 2-PE-HMIL-121, MeNH-HMIL-121, and 1-AP-HMIL-121 were collected and are shown in Figure 3b and c. The ^{13}C CP/MAS NMR spectrum of MIL-121 features three main signals. The signal at ca. 172 ppm arises from the C1 and C2 sites from the Al-coordinated carboxylate and free carboxylic acid groups. The resonances at ca. 134.9 and 130.0 ppm originate from the C3, C4, and C5 sites of phenyl carbons (Figure 3b).[18,32] The less intense signals at ca. 50 ppm belong to residual guest methanol molecules which were subsequently removed during thermal treatment. After the thermolysis procedure is carried out to create hierarchical pores and introduce anhydride functionality, two new resonances appear in the ^{13}C CP/MAS spectrum. The signal at ca. 163.0 ppm is assigned to the anhydride groups formed via condensation of two adjacent free carboxylic acid groups,[33,34] and the other new signal located at ca. 123.2 ppm corresponds to the C6 site, which is formed from the C5 and C4 sites that lost their neighboring carboxylate carbon (i.e., C1 and C2) during decarboxylation under thermal treatment (Figure 3b).

The ^{1}H MAS NMR spectrum of MIL-121 features three resonances (Figure 3c). The resonance at ca. 12 ppm is assigned to the acidic proton on the free COOH groups of the BTEC linker (labeled H1), and the resonance at ca. 8 ppm originates from the phenyl hydrogens (H2) of the BTEC linker. Several proton signals are apparent between 2 and 6 ppm: the broader and weaker resonance is due to the hydroxyl group bridging the adjacent Al centers (H3); the sharper and stronger peak is due to adsorbed methanol. After thermal treatment, the H1 resonance completely disappears owing to the formation of anhydride groups, suggesting that there are no more free carboxylic acid groups inside HMIL-121. As all of the resonances in both ^{13}C and ^{1}H SSNMR spectra in MIL-121 and HMIL-121 are assigned, any new features appearing in the spectra of post-synthetically modified HMIL-121 should originate solely from the new functional moieties introduced during PSM.

In the ^{13}C CP/MAS spectrum of the product obtained from PSM of HMIL-121 via methanol acetylation (termed MeO-MIL-121), there are two new resonances in addition to those seen in the spectrum of the pristine HMIL-121. The signal at ca. 168.5 ppm is assigned to the carbonyl moiety in a phenyl ester, indicating that esterification has occurred between anhydride groups in HMIL-121 and the methanol guests within the pores. The other resonance at ca. 51.0 ppm is due to the methoxy group in the resulting methyl ester. Because MeO-HMIL-121 has been activated at 150 °C under a vacuum for 8 h, the methoxy group signal must exclusively originate from the ester moiety grafted on the MOF, rather than from residual guest methanol. The significant decrease in the intensity of the resonance at ca. 163 ppm due to the anhydride group is also consistent with methanol acetylation. ^{1}H MAS NMR spectra also provide direct evidence of acetylation. Upon reaction with methanol, the H1 resonance reappears, implying that the free carboxylic acid reforms in MeO-HMIL-121 due to esterification (Figure 3c). Together, ^{13}C CP/MAS and ^{1}H MAS SSNMR spectra unambiguously confirm that the esterification of methanol with an anhydride group has occurred inside HMIL-121.

Incorporation of 2-PE (2-phenylethanol), methylamine, and 1-aminopyrene inside HMIL-121 also produced similar spectral features in their respective ^{1}H—^{13}C CP/MAS and ^{1}H

https://dx.doi.org/10.1021/jacs.9b13414
J. Am. Chem. Soc. 2020, 142, 4419−4428

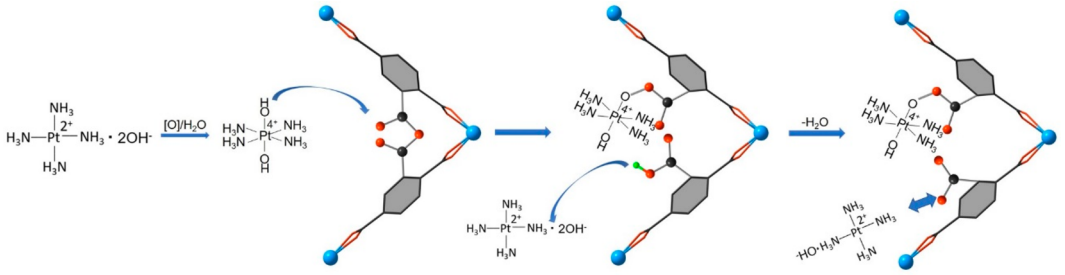

Figure 4. Proposed mechanism of incorporation of the Pt species inside HMIL-121.

MAS NMR spectra, confirming the formation of ester or amide groups and the reformation of free carboxylic acid groups. Other organic molecules including ethanol, aniline, *p*-toluidine, 4-aminobiphenyl, and 1,2-ethanedithiol were also grafted into HMIL-121 via reactions with anhydride groups. The experimental details and results regarding these post-synthetically modified HMIL-121 variants can be found in the Supporting Information.

Modification of HMIL-121 with a Pt Complex. Platinum is one of the most widely used noble metals due to its well-known catalytic properties.[35,36] In contrast to other noble metals, Pt has particularly important pharmaceutical applications, as Pt-based drugs are critical agents for treating several types of cancers.[37,38] Square-planar Pt(II)-based drugs and the more stable carboxylate platinum(IV) prodrugs based on the Pt(II) precursor are used in both research and clinical therapy.[39,40] Carboxylate-functionalized platinum(IV) prodrugs are usually obtained by a reaction between anhydride and square-planar Pt(II) drugs with oxidizing reagents such as O_2, H_2O_2, or Cl_2.[40,41] Keeping these pharmaceutical applications in mind, we have successfully introduced Pt(II) and Pt(IV) species into HMIL-121 using a Pt salt, tetraammineplatinum(II) hydroxide, $Pt(NH_3)_4(OH)_2$, as a precursor. The resulting material is termed as Pt-HMIL-121.

By mixing HMIL-121 with an aqueous solution of $Pt(NH_3)_4(OH)_2$ at room temperature without the need for any catalyst, Pt-HMIL-121 is obtained. The product was collected and washed thoroughly by water to remove any residual Pt precursor (see details in the Supporting Information). To confirm the inclusion of Pt complexes, $^1H-^{195}Pt$ BRAIN-CPMG SSNMR experiments were carried out. This particular NMR technique enables us to acquire extremely wide ^{195}Pt spectra.[23] The experimental and simulated ^{195}Pt NMR spectra of $Pt(NH_3)_4(OH)_2$ and Pt-HMIL-121 are shown in Figure S5a along with a more detailed discussion in the caption (p S12 in the Supporting Information). These $^1H-^{195}Pt$ CP SSNMR experiments reveal the existence of both a Pt(II) and Pt(IV) species in Pt-HMIL-121. The ^{195}Pt SSNMR results are in excellent agreement with XPS analysis (Figure S5b). To further investigate the incorporation of two Pt species in HMIL-121, we also carried out $^1H-^{13}C$ CP/MAS and ^1H MAS SSNMR experiments on Pt-HMIL-121 (Figure S6). As mentioned earlier, the signal at 172 ppm in the ^{13}C spectrum of MIL-121 originates from two overlapping resonances: C1 from the Al-coordinated carbon atom and C2 from the free carboxylate groups. Our previous study[32] showed that, once the free carboxylate groups are doped with extra-framework metal ions, new signals often appear on the lower-field side of the peak at 172 ppm, which is due to the C2 site of the free COO^- group interacting with the newly introduced metal ions. In the ^{13}C spectrum of Pt-HMIL-121, an extra peak indeed appears at ca. 179 ppm as a broad shoulder on the low-field side of the 172 ppm peak (Figure S6a) upon PSM, confirming the HMIL-121 has indeed incorporated Pt. The breadth of the new ^{13}C signal is consistent with ^{195}Pt NMR and XPS results that indicate there is more than one Pt species grafted within the MOF. No H1 resonance is observed in the ^1H MAS spectrum of Pt-HMIL-121 (Figure S6b), which differs from all other HMIL-121 variants modified by organic species, suggesting that the reactions more complicated than simple acetylation involving Pt have taken place.

Based on our multinuclear SSNMR and XPS results, a mechanism can be proposed for this Pt incorporation in HMIL-121. First, Pt(II) in square-planar $Pt(NH_3)_4(OH)_2$ is oxidized to octahedral Pt(IV) by molecular oxygen dissolved in water, resulting in the addition of two hydroxyl groups to the Pt center (Figure 4).[40,41] This octahedral Pt(IV) complex is then bound to a carboxylate group after reacting with an anhydride group of HMIL-121.[41] The incorporation of the octahedral Pt(IV) complex is accompanied by the formation of free carboxylic acid groups that subsequently react with basic $Pt(NH_3)_4(OH)_2$, resulting in grafting the corresponding square-planar Pt(II) species on HMIL-121 (Figure 4). This acid–base reaction is further confirmed by the change in pH during the experiment—the initial aqueous solution of $Pt(NH_3)_4(OH)_2$ has a pH value of 10.0 and gradually becomes neutral after mixing with HMIL-121, providing evidence that a neutralization reaction has occurred. This proposed route also explains the absence of H1 signal in the ^1H MAS NMR spectrum of Pt-HMIL-121 (Figure S6b). The success in incorporation of Pt(II)/Pt(IV) species in the MOF indicates that the PSM protocol described here has potential to be used for drug delivery. More research along this line is needed.

Electrocatalytic Activity toward the ORR. As mentioned earlier, elemental Pt has considerable practical importance in catalysis. Therefore, Pt-HMIL-121 obtained via PSM was used to fabricate a MOF-derived hierarchical porous carbon network with embedded Pt nanoparticles (NPs) as an electrocatalyst for the oxygen reduction reaction (ORR). Fuel cells and metal-air batteries are very promising candidates for environmentally sustainable energy sources, where ORR plays a key role in determining their electrical energy conversion.[42,43] Currently, Pt-based cathodes are still the most efficient materials for catalyzing ORR.[43] Due to the high cost of Pt, developing electrocatalysts of low Pt content without sacrificing performance is critical to achieving large scale industrial production for electric vehicles and other applications involving ORR.[43] Recently, MOF-derived carbon

https://dx.doi.org/10.1021/jacs.9b13414
J. Am. Chem. Soc. 2020, 142, 4419−4428

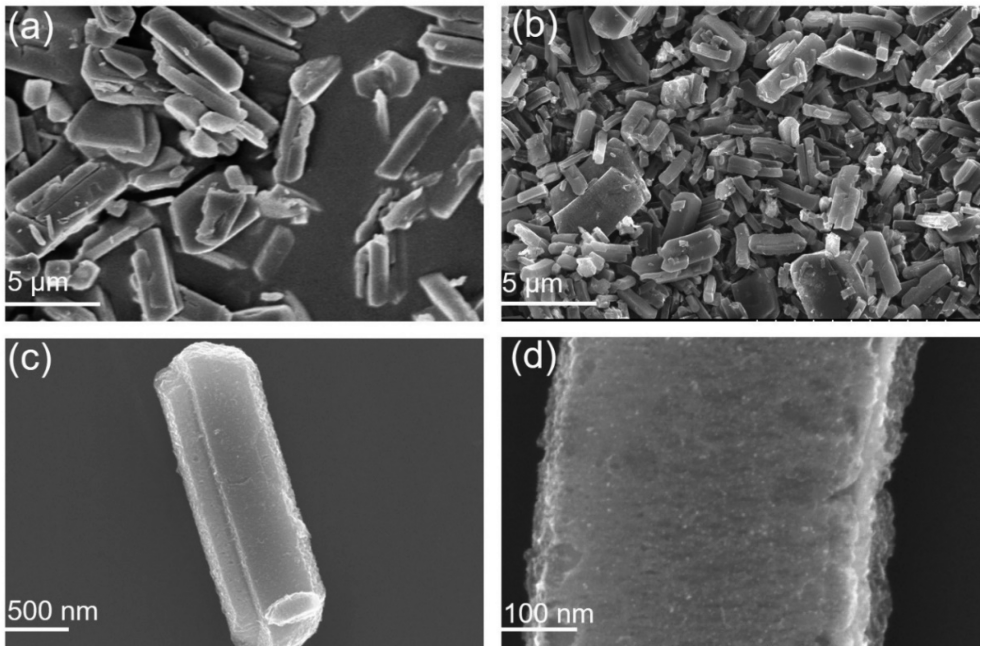

Figure 5. SEM images of Pt-HMIL-121 (a) along with Pt-HMIL-121-900 samples at several different scales (b–d).

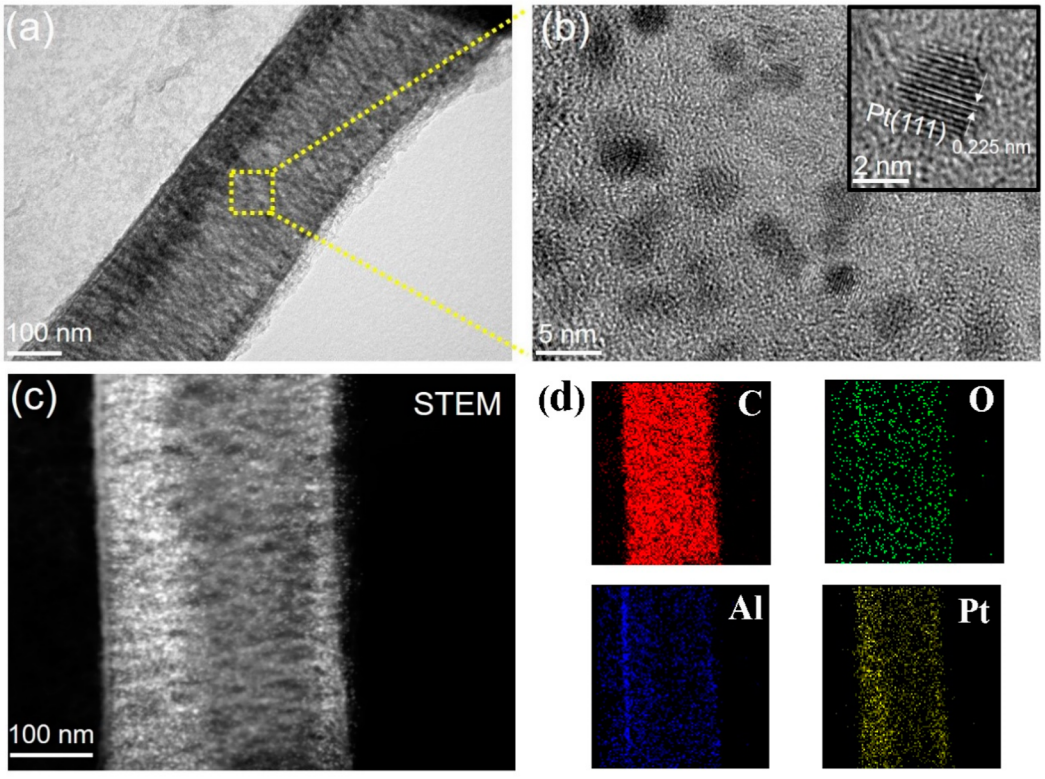

Figure 6. TEM and HRTEM images of Pt-HMIL-121-900. Scale bars are 100 nm in part a, 5 nm in part b, and 2 nm for the inset of part b. The STEM image (c) and element maps (d) of Pt-HMIL-121-900 are also shown.

materials have attracted tremendous attention due to their inherently high surface areas and porosity compared to their parent MOF precursors, leading to high exposure and easy accessibility of the active sites.[11,44] In addition, the resulting MOF-derived carbon materials have much better electrical conductivity and higher thermal/chemical stability compared to their parent MOFs, making them an ideal host for fabricating highly dispersed metal-doped electrocatalysts.[11,45]

Pt-HMIL-121 was pyrolyzed by heat treatment at 900 °C for 1 h under an Ar atmosphere, followed by hydrochloric acid leaching to remove the unstable Al species (see details in the Supporting Information). The resulting catalyst is termed Pt-HMIL-121-900, which is composed of uniformly dispersed Pt nanoparticles embedded in the porous carbon matrix. During pyrolysis, the grafted Pt complexes decompose, generating the reduced metallic Pt NPs. The HMIL-121 substrate is

https://dx.doi.org/10.1021/jacs.9b13414
J. Am. Chem. Soc. 2020, 142, 4419–4428

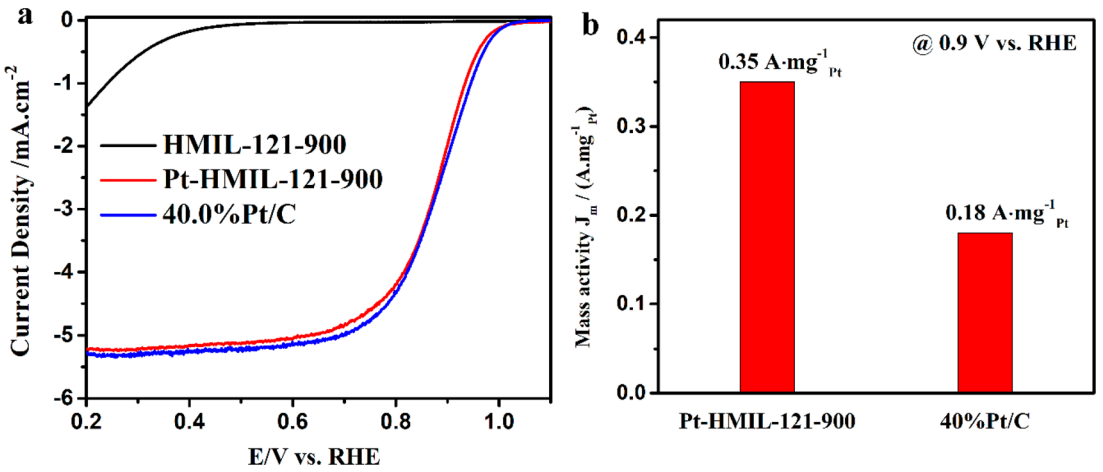

Figure 7. (a) Linear scan voltammogram (LSV) curves for the electrocatalysts of Pt-HMIL-121-900, HMIL-121-900, and 40.0% Pt/C catalysts in O_2-saturated 0.1 M $HClO_4$ solution at room temperature (rotating speed of 1600 rpm, sweep rate of 10 mV·s^{-1}). (b) The mass activity at 0.9 V (vs RHE) for Pt-HMIL-121-900 and commercial 40% Pt/C catalysts.

carbonized and converted into the conductive Al-doped porous carbon. The Pt-HMIL-121-900 material with highly dispersed Pt NPs was thus fabricated. Before testing the electrochemical catalytic performance, the morphology of the precursor (Pt-HMIL-121) and the catalyst (Pt-HMIL-121-900) was carefully examined by scanning electron microscopy (SEM). As shown in Figure 5, the SEM images at different scales indicate that Pt-HMIL-121-900 remains as parallele-piped-shaped crystals, which are similar to those of parent Pt-HMIL-121. After high-temperature treatment at 900 °C, the Pt-HMIL-121-900 crystal sizes became smaller than those of HMIL-121 (Figures S1d and 5a,b), which is a common phenomenon in carbonized MOFs due to the loss of most H and O elements.[46] The crystal faces of Pt-HMIL-121-900 are decorated with prominent mesopores, suggesting the existence of a hierarchical structure with a large average pore size. The differences in surface area and hierarchical pores between Pt-HMIL-121 and Pt-HMIL-121-900 were further characterized by N_2 sorption tests. The two samples both show the same type IV isotherms with hysteresis loops, which are similar to that of HMIL-121 (Figure S7), suggesting the existence of both mesopores and micropores. The calculated BET surface area for Pt-HMIL-121 is 411.0 m^2/g, which is less than that of HMIL-121 (887.6 m^2/g) due to the steric hindrance of the incorporated Pt complex species within the pore channels. In contrast, the BET surface area for Pt-HMIL-121-900 reaches as high as 2866 m^2/g. This value is one of the highest reported BET surface areas among pyrolytic MOFs,[45,47] suggesting Pt-HMIL-121-900 has potential to provide sufficient exposure of the Pt sites, which can facilitate mass transport during the ORR.

Transmission electron microscopy (TEM) images show more details of the Pt-HMIL-121-900 sample. From Figure 6a, it can be seen that Pt-HMIL-121 is converted into an Al-doped porous carbon network decorated with Pt NPs dispersed both on the surface and in the pores of the Pt-HMIL-121-900 substrate. The high-resolution TEM image clearly shows uniform Pt particles with an average size of 2.5 nm (Figure 6b), suggesting that the Pt particle size is controlled by the nanopore trapping effect, which prevents Pt NPs from diffusion and therefore aggregation during heating. The lattice distance of crystalline Pt NPs is measured from the HRTEM image and given in the inset of Figure 6b. The periodic fringe spaces are 0.225 nm, which agrees well with the interplanar *d* value for (111) planes of crystalline Pt.[48] Elemental mapping analysis (Figure 6c,d) demonstrates that Pt-HMIL-121-900 is composed of C, O, Al, and Pt, with Pt and Al well dispersed in the porous carbon matrix. The Pt loading determined by ICP-OES is 7.0 wt % of Pt in Pt-HMIL-121-900. The PXRD patterns of Pt-HMIL-121 and Pt-HMIL-121-900 have significant differences and are shown in Figure S8. After pyrolysis, the diffraction peaks of HMIL-121 disappear, and well-defined crystalline Pt reflections appear in the PXRD pattern of Pt-HMIL-121-900 (Figure S8). The porous carbon is generated from the decomposition of the host HMIL-121. During high-temperature pyrolysis, most of the hydrogen, oxygen, and carbon elements are vaporized, resulting in a Pt-doped hierarchically porous carbon material.

The electrochemical performance of Pt-HMIL-121-900 has been evaluated for ORR and compared with the performances of pyrolytic HMIL-121 (termed as HMIL-121-900) and the state-of-the-art commercial Pt/C catalyst (40.0 wt % Pt and termed as 40% Pt/C catalyst). Figure 7a presents the linear scan voltammogram (LSV) curves for Pt-HMIL-121-900, HMIL-121-900, and 40% Pt/C catalysts obtained in a O_2-saturated 0.1 M $HClO_4$ electrolyte at a rotating speed of 1600 rpm. Pt-HMIL-121-900 displays a significantly positively shifted ORR onset potential of 1.04 V (vs RHE) and a higher current density of 5.3 mA·cm^{-2} compared to the corresponding values of HMIL-121-900. The kinetic currents at 0.9 V for the studied electrocatalysts obtained from the Koutecky–Levich equation were used to derive Pt mass activities (Figure 7b). For the fresh catalysts, Pt-HMIL-121-900 exhibits a mass activity of 0.35 A·mg$_{Pt}^{-1}$ at 0.9 V, which is about 2 times higher than that of commercial 40% Pt/C catalyst (0.18 A·mg$_{Pt}^{-1}$). The result indicates that Pt-HMIL-121-900 with an ultralow Pt loading of 7.0 wt % exhibits excellent catalytic performance in the ORR and has a much higher ORR mass activity compared to that of the commercial Pt/C catalyst. The combination of highly dispersed Pt NPs with appropriate particle sizes and the hierarchically porous carbon matrix (Pt-HMIL-121-900) derived from MOF-based material results in an excellent ORR activity. This work demonstrates that the hierarchically porous HMIL-121 MOF functionalized with anhydride groups has great potential for fabrication of efficient Pt-doped

https://dx.doi.org/10.1021/jacs.9b13414
J. Am. Chem. Soc. 2020, 142, 4419−4428

electrocatalysts for ORR as well as for other energy conversion reactions involving Pt metal.

CONCLUSION

In this work, we have demonstrated that a hierarchically porous MOF decorated with anhydride groups is a novel platform for PSM of MOFs. It exhibits excellent reactivity toward covalently grafting various organic species as well as Pt(IV)/Pt(II) complexes on the pore walls. The ability of this protocol to immobilize Pt(II)/Pt(IV) species inside MOFs has important implications for drug delivery and fabrication of Pt-based heterogeneous catalysts. The combination of the highly active anhydride group and the hierarchical pore structure of the MOF makes the approach described a novel and very effective protocol for PSM of MOFs. This strategy opens a novel avenue for introducing multiple chemical functionalities inside MOFs and also offers a tunable platform for metalation of MOFs with noble metals. Furthermore, the fact that the precursor for PSM (i.e., the hierarchically porous MOF decorated with anhydride groups) can be easily prepared from simple low-cost carboxylate-based MOFs via thermolysis in a controlled fashion and that, in addition to MIL-121, many important MOFs either have or can be easily functionalized to form free carboxylic acid groups make this new PSM method widely applicable for diverse applications. Looking forward, covalent organic frameworks (COFs) can be functionalized via carboxylic groups,[49,50] which suggests that the protocol described here can be expanded to include PSM of COFs and other related porous organic polymers.

ASSOCIATED CONTENT

Supporting Information

The Supporting Information is available free of charge at https://pubs.acs.org/doi/10.1021/jacs.9b13414.

Details on sample preparation, additional PXRD patterns, SEM images, N_2 adsorption isotherms, ^{13}C CP/MAS and ^{1}H MAS spectra, $^{1}H-^{195}Pt$ BRAIN-CPMG SSNMR spectra and ^{195}Pt CS tensor parameters, and XPS and TGA data (PDF)

AUTHOR INFORMATION

Corresponding Authors

Xueliang Sun − *Department of Mechanical and Materials Engineering, The University of Western Ontario, London, Ontario, Canada N6A 5B9;* orcid.org/0000-0003-0374-1245; Email: xsun@eng.uwo.ca

Yining Huang − *Department of Chemistry, The University of Western Ontario, London, Ontario, Canada N6A 5B7;* orcid.org/0000-0001-9265-5896; Email: yhuang@uwo.ca

Authors

Shoushun Chen − *Department of Chemistry, The University of Western Ontario, London, Ontario, Canada N6A 5B7*

Zhongxin Song − *Department of Mechanical and Materials Engineering, The University of Western Ontario, London, Ontario, Canada N6A 5B9; College of Materials Science and Engineering, Shenzhen University, Shenzhen 518060, China*

Jinghui Lyu − *Department of Chemistry, The University of Western Ontario, London, Ontario, Canada N6A 5B7; College of Chemical Engineering, Zhejiang University of Technology, State Key Laboratory Breeding Base of Green Chemistry Synthesis Technology, Hangzhou, PR China 310032*

Ying Guo − *Department of Chemistry, The University of Western Ontario, London, Ontario, Canada N6A 5B7; State Key Laboratory of Chemical Resource Engineering, Beijing University of Chemical Technology, Beijing, PR China 100029*

Bryan E. G. Lucier − *Department of Chemistry, The University of Western Ontario, London, Ontario, Canada N6A 5B7;* orcid.org/0000-0002-9682-4324

Wilson Luo − *Department of Chemistry, The University of Western Ontario, London, Ontario, Canada N6A 5B7*

Mark S. Workentin − *Department of Chemistry, The University of Western Ontario, London, Ontario, Canada N6A 5B7;* orcid.org/0000-0001-8517-6483

Complete contact information is available at: https://pubs.acs.org/10.1021/jacs.9b13414

Author Contributions

#S.C. and Z.S. contributed equally to this work.

Notes

The authors declare no competing financial interest.

ACKNOWLEDGMENTS

Y.H., X.S., and M.S.W. thank the Natural Science and Engineering Research Council (NSERC) of Canada for Discovery Grants. X.S. also thanks Canada Research Chair (CRC) Program, Canada Foundation for Innovation (CFI), and Ontario Research Fund (ORF). The National Natural Science Foundation of China is acknowledged by Z.S. (NSFC21905179), J.L. (NSFC21506189), and Y.G. (NSFC51472021).

REFERENCES

(1) Furukawa, H.; Cordova, K. E.; O'Keeffe, M.; Yaghi, O. M. The chemistry and applications of metal-organic frameworks. *Science* **2013**, *341* (6149), 1230444.

(2) Zhou, H.-C.; Long, J. R.; Yaghi, O. M. Introduction to Metal−Organic Frameworks. *Chem. Rev.* **2012**, *112* (2), 673−674.

(3) Chen, M.; Chen, S.; Chen, W.; Lucier, B. E. G.; Zhang, Y.; Zheng, A.; Huang, Y. Analyzing Gas Adsorption in an Amide-Functionalized Metal Organic Framework: Are the Carbonyl or Amine Groups Responsible? *Chem. Mater.* **2018**, *30* (11), 3613−3617.

(4) Yu, J.; Xie, L.-H.; Li, J.-R.; Ma, Y.; Seminario, J. M.; Balbuena, P. B. CO_2 capture and separations using MOFs: computational and experimental studies. *Chem. Rev.* **2017**, *117* (14), 9674−9754.

(5) Park, T.-H.; Hickman, A. J.; Koh, K.; Martin, S.; Wong-Foy, A. G.; Sanford, M. S.; Matzger, A. J. Highly dispersed palladium (II) in a defective metal−organic framework: application to C−H activation and functionalization. *J. Am. Chem. Soc.* **2011**, *133* (50), 20138−20141.

(6) Jiang, H.-L.; Akita, T.; Ishida, T.; Haruta, M.; Xu, Q. Synergistic catalysis of Au@Ag core−shell nanoparticles stabilized on metal−organic framework. *J. Am. Chem. Soc.* **2011**, *133* (5), 1304−1306.

(7) Dhakshinamoorthy, A.; Garcia, H. Catalysis by metal nanoparticles embedded on metal−organic frameworks. *Chem. Soc. Rev.* **2012**, *41* (15), 5262−5284.

(8) Hu, Z.; Deibert, B. J.; Li, J. Luminescent metal−organic frameworks for chemical sensing and explosive detection. *Chem. Soc. Rev.* **2014**, *43* (16), 5815−5840.

(9) Horcajada, P.; Serre, C.; Vallet-Regí, M.; Sebban, M.; Taulelle, F.; Férey, G. Metal−organic frameworks as efficient materials for drug delivery. *Angew. Chem.* **2006**, *118* (36), 6120−6124.

(10) Horcajada, P.; Chalati, T.; Serre, C.; Gillet, B.; Sebrie, C.; Baati, T.; Eubank, J. F.; Heurtaux, D.; Clayette, P.; Kreuz, C. Porous metal-organic-framework nanoscale carriers as a potential platform for drug delivery and imaging. *Nat. Mater.* **2010**, *9* (2), 172.

(11) Zhao, Y.; Song, Z.; Li, X.; Sun, Q.; Cheng, N.; Lawes, S.; Sun, X. Metal organic frameworks for energy storage and conversion. *Energy Storage Mater.* **2016**, *2*, 35−62.
(12) Jiang, J.; Zhao, Y.; Yaghi, O. M. Covalent chemistry beyond molecules. *J. Am. Chem. Soc.* **2016**, *138* (10), 3255−3265.
(13) Cohen, S. M. The postsynthetic renaissance in porous solids. *J. Am. Chem. Soc.* **2017**, *139* (8), 2855−2863.
(14) Cohen, S. M. Postsynthetic methods for the functionalization of metal−organic frameworks. *Chem. Rev.* **2012**, *112* (2), 970−1000.
(15) Moghadam, P. Z.; Li, A.; Wiggin, S. B.; Tao, A.; Maloney, A. G.; Wood, P. A.; Ward, S. C.; Fairen-Jimenez, D. Development of a Cambridge Structural Database subset: a collection of metal−organic frameworks for past, present, and future. *Chem. Mater.* **2017**, *29* (7), 2618−2625.
(16) Evans, J. D.; Sumby, C. J.; Doonan, C. J. Post-synthetic metalation of metal−organic frameworks. *Chem. Soc. Rev.* **2014**, *43* (16), 5933−5951.
(17) Carey, F. A.; Sundberg, R. J. *Advanced organic chemistry: part A: structure and mechanisms*; Springer Science & Business Media: 2007.
(18) Volkringer, C.; Loiseau, T.; Guillou, N.; Férey, G. r.; Haouas, M.; Taulelle, F.; Elkaim, E.; Stock, N. High-Throughput Aided Synthesis of the Porous Metal− Organic Framework-Type Aluminum Pyromellitate, MIL-121, with Extra Carboxylic Acid Functionalization. *Inorg. Chem.* **2010**, *49* (21), 9852−9862.
(19) Chen, S.; Mukherjee, S.; Lucier, B. E.; Guo, Y.; Wong, Y. T. A.; Terskikh, V. V.; Zaworotko, M. J.; Huang, Y. Cleaving Carboxyls: Understanding Thermally Triggered Hierarchical Pores in the Metal-Organic Framework MIL-121. *J. Am. Chem. Soc.* **2019**, *141* (36), 14257−14271.
(20) Hayashi, S.; Hayamizu, K. Shift references in high-resolution solid-state NMR. *Bull. Chem. Soc. Jpn.* **1989**, *62* (7), 2429−2430.
(21) Hayashi, S.; Hayamizu, K. Chemical shift standards in high-resolution solid-state NMR (1) ^{13}C, ^{29}Si, and ^{1}H nuclei. *Bull. Chem. Soc. Jpn.* **1991**, *64* (2), 685−687.
(22) Harris, R. K.; Becker, E. D.; Cabral de Menezes, S. M.; Goodfellow, R.; Granger, P. NMR nomenclature. Nuclear spin properties and conventions for chemical shifts (IUPAC recommendations 2001). *Pure Appl. Chem.* **2001**, *73* (11), 1795−1818.
(23) Harris, K. J.; Lupulescu, A.; Lucier, B. E.; Frydman, L.; Schurko, R. W. Broadband adiabatic inversion pulses for cross polarization in wideline solid-state NMR spectroscopy. *J. Magn. Reson.* **2012**, *224*, 38−47.
(24) Tang, J. A.; O'Dell, L. A.; Aguiar, P. M.; Lucier, B. E.; Sakellariou, D.; Schurko, R. W. Application of static microcoils and WURST pulses for solid-state ultra-wideline NMR spectroscopy of quadrupolar nuclei. *Chem. Phys. Lett.* **2008**, *466* (4), 227−234.
(25) O'Dell, L. A. The WURST kind of pulses in solid-state NMR. *Solid State Nucl. Magn. Reson.* **2013**, *55*, 28−41.
(26) Mayrhofer, K.; Strmcnik, D.; Blizanac, B.; Stamenkovic, V.; Arenz, M.; Markovic, N. Measurement of oxygen reduction activities via the rotating disc electrode method: From Pt model surfaces to carbon-supported high surface area catalysts. *Electrochim. Acta* **2008**, *53* (7), 3181−3188.
(27) Lucier, B. E. G.; Chen, S.; Huang, Y. Characterization of Metal−Organic Frameworks: Unlocking the Potential of Solid-State NMR. *Acc. Chem. Res.* **2018**, *51* (2), 319−330.
(28) Chen, S.; Lucier, B. E. G.; Boyle, P. D.; Huang, Y. Understanding The Fascinating Origins of CO_2 Adsorption and Dynamics in MOFs. *Chem. Mater.* **2016**, *28* (16), 5829−5846.
(29) Morris, W.; Doonan, C. J.; Yaghi, O. M. Postsynthetic modification of a metal−organic framework for stabilization of a hemiaminal and ammonia uptake. *Inorg. Chem.* **2011**, *50* (15), 6853−6855.
(30) Ahnfeldt, T.; Gunzelmann, D.; Loiseau, T.; Hirsemann, D.; Senker, J. r.; Férey, G.; Stock, N. Synthesis and modification of a functionalized 3D open-framework structure with MIL-53 topology. *Inorg. Chem.* **2009**, *48* (7), 3057−3064.
(31) Otera, J.; Nishikido, J. *Esterification: methods, reactions, and applications*; John Wiley & Sons: 2009.
(32) Chen, S.; Lucier, B. E. G.; Luo, W.; Xie, X.; Feng, K.; Chan, H.; Terskikh, V. V.; Sun, X.; Sham, T.-K.; Workentin, M. S. Loading across the Periodic Table: Introducing 14 Different Metal Ions To Enhance Metal−Organic Framework Performance. *ACS Appl. Mater. Interfaces* **2018**, *10* (36), 30296−30305.
(33) Ragon, F.; Campo, B.; Yang, Q.; Martineau, C.; Wiersum, A. D.; Lago, A.; Guillerm, V.; Hemsley, C.; Eubank, J. F.; Vishnuvarthan, M. Acid-functionalized UiO-66 (Zr) MOFs and their evolution after intra-framework cross-linking: structural features and sorption properties. *J. Mater. Chem. A* **2015**, *3* (7), 3294−3309.
(34) Reimer, N.; Gil, B.; Marszalek, B.; Stock, N. Thermal post-synthetic modification of Al-MIL-53−COOH: systematic investigation of the decarboxylation and condensation reaction. *CrystEngComm* **2012**, *14* (12), 4119−4125.
(35) Periana, R. A.; Taube, D. J.; Gamble, S.; Taube, H.; Satoh, T.; Fujii, H. Platinum catalysts for the high-yield oxidation of methane to a methanol derivative. *Science* **1998**, *280* (5363), 560−564.
(36) Labinger, J. A. Platinum-catalyzed C−H functionalization. *Chem. Rev.* **2017**, *117* (13), 8483−8496.
(37) Zheng, Y.-R.; Suntharalingam, K.; Johnstone, T. C.; Lippard, S. J. Encapsulation of Pt (IV) prodrugs within a Pt (II) cage for drug delivery. *Chem. Sci.* **2015**, *6* (2), 1189−1193.
(38) Wong, E.; Giandomenico, C. M. Current status of platinum-based antitumor drugs. *Chem. Rev.* **1999**, *99* (9), 2451−2466.
(39) Yap, S. Q.; Chin, C. F.; Thng, H.; Hwee, A.; Pang, Y. Y.; Ho, H. K.; Ang, W. H. Finely Tuned Asymmetric Platinum (IV) Anticancer Complexes: Structure−Activity Relationship and Application as Orally Available Prodrugs. *ChemMedChem* **2017**, *12* (4), 300−311.
(40) Wilson, J. J.; Lippard, S. J. Synthetic methods for the preparation of platinum anticancer complexes. *Chem. Rev.* **2014**, *114* (8), 4470−4495.
(41) Chin, C. F.; Tian, Q.; Setyawati, M. I.; Fang, W.; Tan, E. S. Q.; Leong, D. T.; Ang, W. H. Tuning the activity of platinum (IV) anticancer complexes through asymmetric acylation. *J. Med. Chem.* **2012**, *55* (17), 7571−7582.
(42) Dai, L.; Xue, Y.; Qu, L.; Choi, H.-J.; Baek, J.-B. Metal-free catalysts for oxygen reduction reaction. *Chem. Rev.* **2015**, *115* (11), 4823−4892.
(43) Nie, Y.; Li, L.; Wei, Z. Recent advancements in Pt and Pt-free catalysts for oxygen reduction reaction. *Chem. Soc. Rev.* **2015**, *44* (8), 2168−2201.
(44) Cao, X.; Tan, C.; Sindoro, M.; Zhang, H. Hybrid micro-/nanostructures derived from metal−organic frameworks: preparation and applications in energy storage and conversion. *Chem. Soc. Rev.* **2017**, *46* (10), 2660−2677.
(45) Liang, Z.; Qu, C.; Xia, D.; Zou, R.; Xu, Q. Atomically dispersed metal sites in MOF-based materials for electrocatalytic and photocatalytic energy conversion. *Angew. Chem., Int. Ed.* **2018**, *57*, 9604−9633.
(46) Zhang, H.; Hwang, S.; Wang, M.; Feng, Z.; Karakalos, S.; Luo, L.; Qiao, Z.; Xie, X.; Wang, C.; Su, D. Single atomic iron catalysts for oxygen reduction in acidic media: particle size control and thermal activation. *J. Am. Chem. Soc.* **2017**, *139* (40), 14143−14149.
(47) Indra, A.; Song, T.; Paik, U. Metal organic framework derived materials: Progress and prospects for the energy conversion and storage. *Adv. Mater.* **2018**, *30* (39), 1705146.
(48) Guo, X.; Li, L.; Zhang, X.; Chen, J. Platinum Nanoparticles Encapsulated in Nitrogen-Doped Mesoporous Carbons as Methanol-Tolerant Oxygen Reduction Electrocatalysts. *ChemElectroChem* **2015**, *2* (3), 404−411.
(49) Lu, Q.; Ma, Y.; Li, H.; Guan, X.; Yusran, Y.; Xue, M.; Fang, Q.; Yan, Y.; Qiu, S.; Valtchev, V. Postsynthetic Functionalization of Three-Dimensional Covalent Organic Frameworks for Selective Extraction of Lanthanide Ions. *Angew. Chem., Int. Ed.* **2018**, *57* (21), 6042−6048.
(50) Guo, L.; Jia, S.; Diercks, C. S.; Yang, X.; Alshmimri, S. A.; Yaghi, O. M. Amidation, Esterification, and Thioesterification of a Carboxyl-Functionalized Covalent Organic Framework. *Angew. Chem., Int. Ed.* **2020**, *59* (5), 2023−2027.

https://dx.doi.org/10.1021/jacs.9b13414
J. Am. Chem. Soc. 2020, 142, 4419−4428